Journal of Materials Chemistry C

ROYAL SOCIETY OF CHEMISTRY

PAPER

View Article Online
View Journal | View Issue

Cite this: J. Mater. Chem. C, 2024, 12, 1668

High-performance top-emitting quantum dot light-emitting diodes by balancing electrical conductance and light outcoupling†

Weigao Wang,[ab] Zhenghui Wu,[c] Guanding Mei,[c] Jingrui Ma,[c] Hua An,[ab] Kai Wang,[cd] Xiao Wei Sun *[cd] and Zhengchun Peng *[ab]

We present a method for fabricating top-emitting quantum dot light-emitting diodes (TE-QLEDs) with high performance through a solution-based process. The ITO as an interfacial layer can effectively improve the hydrophilicity of the glass substrate/Al, addressing the difficulty in depositing a smooth poly(3,4-ethylenedioxythiophene) polystyrene sulfonate (PEDOT:PSS) film on the Al electrode. Additionally, the ITO layer also reduces the barrier of hole injection between the glass substrate/Al and the PEDOT:PSS film. Simulation reveals that the wide-angle interference in the normal direction becomes destructive as the ITO thickness increases. The waveguide mode confines more photons and inhibits the light outcoupling, thus decreasing the efficiency of the TE-QLEDs. By balancing electrical conductance and light outcoupling, an optimized performance is achieved at an ITO layer thickness of 5 nm. The red-emitting TE-QLEDs exhibit a maximum luminance and external quantum efficiency of 175 000 cd m^{-2} and 20.1%, respectively. The consistency between the experimental data and the simulation results supports the significance of the ITO thickness in determining the device's efficiency. This study provides important insight into the preparation of high-performance TE-QLEDs through the interfacial modification of the metal oxides.

Received 17th October 2023,
Accepted 10th December 2023

DOI: 10.1039/d3tc03780k

rsc.li/materials-c

Introduction

Semiconducting colloidal quantum dots (QDs) have attracted great interests owing to their exceptional optoelectronic properties, such as high photoluminescence (PL) quantum yield, narrow linewidth, low-cost solution process, and tunable emission wavelength by controlling the size of QDs. Quantum dot light-emitting diodes (QLEDs) have emerged as a promising technology for displays and solid-state lighting, due to their unique advantages.[1–9] With rapid progresses in QLEDs, their performance especially the external quantum efficiency (EQE) has reached the theoretical limit of about 20%.[10–14] The excellent performance has further promoted the development of QLEDs for commercialization, especially the solution-processed QLEDs.

At present, the conventional bottom-emitting structures have been widely employed for QLEDs, which emit light through the glass substrate. This would limit the aperture ratio of pixels for display and restrict the devices to transparent substrates. On the contrary, top-emitting architectures could effectively contribute to high aperture ratios, because the light in each pixel could be emitted from the top electrode without being hindered by the driving circuit elements.[15] Moreover, the top-emitting (TE) device also expands the selection of substrate materials that even include opaque or flexible substrates.[16] So far, although some TE-QLEDs have been reported to exhibit high efficiency, they often require the use of organic functional materials as hole transport layers (HTL) or electron transport layers (ETL).[17–21] This reliance on expensive vacuum equipments deviates from the all solution-based process. In contrast, the solution-process approaches including ink printing, spin-coating, spray-coating, *etc.*, are beneficial for low-cost deposition of large-area and flexible thin films, which is also one of the main advantages of QLEDs.[22] The hydrophilicity to the substrate in solution processing limits the selection of substrates.[23] Usually, metallic materials including silver (Ag) and aluminum (Al),

[a] State Key Laboratory of Radio Frequency Heterogeneous Integration, Shenzhen University, Shenzhen, Guangdong, 518060, China. E-mail: zcpeng@szu.edu.cn
[b] Key Laboratory of Optoelectronic Devices and Systems of Ministry of Education and Guangdong Province, School of Physics and Optoelectronic Engineering, Shenzhen University, Shenzhen, Guangdong, 518060, China
[c] Institute of Nanoscience and Applications, and Department of Electrical and Electronic Engineering, Southern University of Science and Technology, Shenzhen, Guangdong, 518055, China. E-mail: sunxw@sustech.edu.cn
[d] Key Laboratory of Energy Conversion and Storage Technologies (Southern University of Science and Technology), Ministry of Education, and Shenzhen Key Laboratory for Advanced Quantum Dot Displays and Lighting, Southern University of Science and Technology, Shenzhen, Guangdong, 518055, China

† Electronic supplementary information (ESI) available. See DOI: https://doi.org/10.1039/d3tc03780k

are applied as the bottom electrode in TE-QLEDs because they have high reflectivity in the visible range and suitable energy levels that match the charge transport layer.[17,18] Nevertheless, the thermal evaporation of the Ag electrode results in a rougher surface than that of the Al electrode. This can lead to the formation of small and sharp silver grains on the substrate, which can influence the following film formation of the device.[24] On the other hand, the deposition of a homogeneous film over the Al bottom electrode by solution process is especially difficult due to the poor surface wettability of the Al film, which will affect the morphology of the subsequent functional layers.[25] If the Al electrode is subjected to surface cleaning treatment like ultraviolet-ozone (UVO) to improve the surface hydrophilicity, it would generate adverse metal oxides on the surface and inconsistent surface properties between Al and oxides.

Generally, in order to improve the performance of TE-QLEDs by solution process, the interfacial modification layer is applied to minimize the charge injection barrier between the electrode and the hole injection layer (HIL). At the same time, the interface layer can also improve the surface wettability of the Al electrode without the generation of insulating oxides during the surface cleaning treatments. The anode interfacial modification layer should be selected reasonably to improve hole injection and maintain the long-term reliability of devices. It's worth noting that various inorganic transition metal oxides are utilized as hole injection interfacial modification layers to enhance hole injection through suitable energy levels, such as nickel oxide (NiO_x), vanadium oxide (V_2O_5), tungsten oxide (WO_3) and molybdenum oxide (MoO_3).[26,27] For example, Jiang *et al.*[28] conducted thermal evaporation of a MoO_3 thin film instead of PEDOT:PSS over Al electrode, the EQE of TE-QLEDs reached 6.4% due to improved hole injection by MoO_3 film. Thereafter, Tang *et al.*[29] reported a solution-processed MoO_3 film as the HTL deposited on top of Al electrode to manufacture high-performance green emitting TE-QLEDs, whose EQE was as high as 7.4%. Our group[30] has applied indium tin oxide (ITO), MoO_3 and NiO_x as the interface modification layer to improve the wettability of the Al electrode and reduce the hole injection barrier with appropriate energy levels at the metal/organic interface. The red TE-QLEDs demonstrated a maximum EQE of 11.8% with an ITO interlayer. However, our previous study did not give enough consideration to the impact of ITO layer thickness on the light outcoupling. In this work, we further significantly improve the device by taking the microcavity effect into account.

Here we find that the ITO interface modification layer can improve the wettability of the Al electrode, so that the PEDOT:PSS film exhibits a flat, continuous surface on the glass substrate/Al, facilitating the charge injection of devices. Simultaneously, the cavity length of the device varies with the thickness of the ITO interlayer, which can significantly enhance the optical properties of the devices. As observed in the experimental investigation, the efficiency of TE-QLED is highly dependent on the cavity length, which corresponds to the theoretical analyses with a rigorous electromagnetic simulation model. Consequently, when the ITO interlayer is 5 nm, the TE-QLEDs show the maximum luminance and EQE of the TE-QLEDs are 175 000 cd m^{-2} and 20.1%, respectively, which is twice that of the device without an ITO layer. These performance enhancements are mainly attributed to the optimal strategy between charge injection balance and light outcoupling by optimizing the thickness of the ITO interfacial layer. Our method provides feasible guidelines for high-performance TE-QLEDs by solution-processed.

Results and discussion

Fig. 1a shows the schematic structure of the TE-QLEDs with glass/Al/ITO/PEDOT:PSS/TFB/QDs/ZnMgO:PVP/ITO. The corresponding cross-sectional scanning electron microscopy (SEM) image of the device based on the ITO interlayer is shown in Fig. 1b, from which an orderly multilayer structure could be clearly observed. To address the microcavity effect from TE-QLEDs, we use the highly transparent ITO as the top electrode to decrease light reflection and enhance the light outcoupling. The transmittance of the 80 nm ITO cathode on top is $\approx$93% at 630 nm as shown in Fig. S1 (ESI†). To protect the QDs from being damaged during the sputtering of ITO electrodes, a composite buffer layer was introduced consisting of ZnMgO nanoparticles and polyvinylpyrrolidone (PVP).[31,32] In addition, the work function (WF) of the ITO interlayer was investigated by ultraviolet photon spectroscopy (UPS). As we can see in Fig. 1d and e, the WF with the 5 and 10 nm of the ITO interlayer is estimated to be −4.9 eV, which is the same as that of 15 nm ITO interlayer as our earlier report.[30] According to the energy level alignment of the device (Fig. 1c), there exists a large energy barrier of about 1 eV between the WF of the Al anode (−4.2 eV) and HIL of the PEDOT:PSS (−5.2 eV).[10,29] It is difficult for holes to be injected from the anode into the QD layer of the TE-QLEDs. However, the introduced interface modification layer ITO on the Al bottom electrodes can effectively reduce the hole injection barrier between Al and PEDOT:PSS film, and improve the hole injection by the cascade energy alignment.

The commercialized PEDOT:PSS materials possessing excellent hole-injection properties can work as the HIL in QLEDs and spin-coating fabrication of PEDOT:PSS on the ITO substrate is usually adopted.[33] Nevertheless, a major difficulty in preparing the TE-QLEDs is depositing a uniform film of PEDOT:PSS over the Al electrode by spin-coating. Due to its aqueous nature, the PEDOT:PSS has low wettability on the surface of the Al film. As a representative transparent conducting oxide, ITO has been widely used in photoelectric devices for its excellent conductivity and stability, the surface of which could be subjected to various surface cleaning treatments.[34] Hence, the ITO film as the interface modification layer was deposited on the Al electrode, which can effectively improve the surface properties of the Al. To investigate the hydrophilicity of the ITO interlayer, the contact angles of PEDOT:PSS solution on the Al electrode with and without ITO layer were measured after UVO treatment for 30 s. Fig. 2 exhibits the change of contact angles of PEDOT:PSS solution on the Al layer with/without the ITO interlayer. The contact angle of the Al electrode without the ITO interlayer is

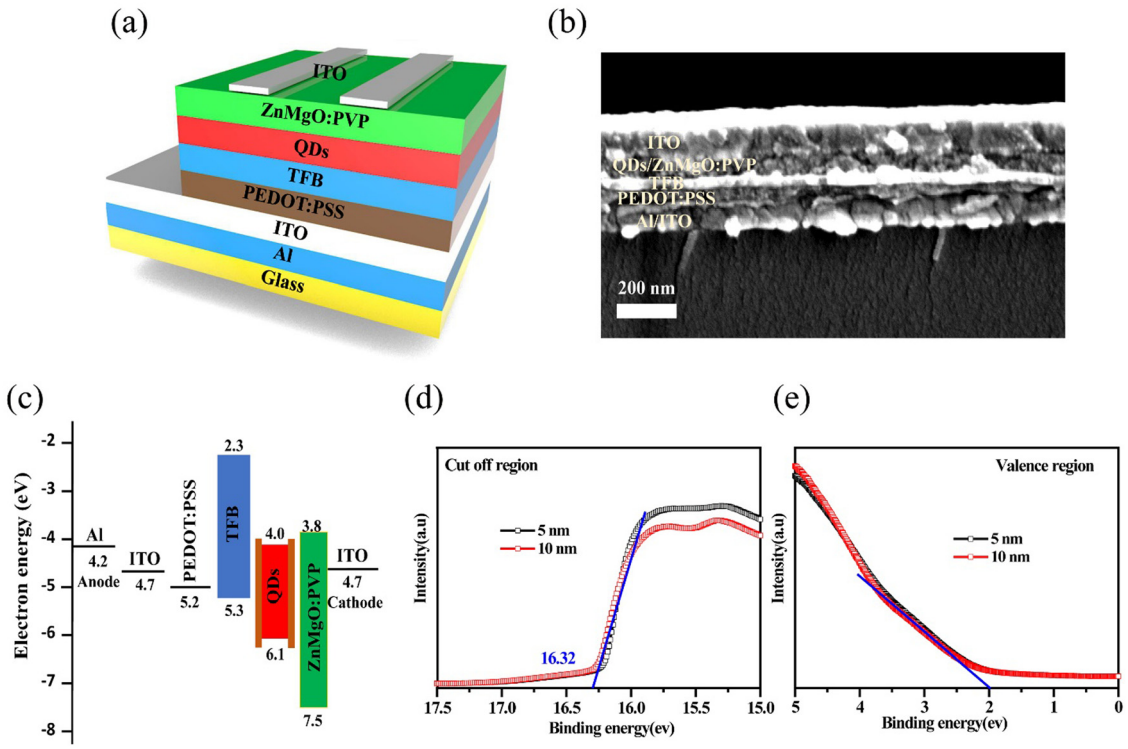

Fig. 1 (a) Device structure, (b) cross-sectional SEM image, and (c) energy level diagram of the TE-QLEDs. (d) Secondary-electron cut-off and (e) valence band edge regions of the ITO films with thickness of 5 nm and 10 nm.

about 57° as shown in Fig. 2a, which means a poor hydrophilicity property of the aqueous solution on the Al film. The contact angle reduces from 48° to 31° when the thickness of ITO interface modification layer increases from 5 nm to 15 nm (Fig. 2b–d), suggesting a good hydrophilicity of the Al electrode with ITO interlayer. When the thickness of the ITO interlayer exceeds 20 nm (Fig. 2e and f), the contact angle increases slightly, which may be caused by the rough surface of the ITO layer. Nonetheless, the surface property of the Al electrode can be effectively modified after depositing the ITO modification layer, which facilitates the formation of a homogeneous PEDOT:PSS film.

In addition, the ITO interlayer could effectively improve the surface morphology of the following functional layers by solution processing. Atomic force microscopy (AFM) was utilized to measure the surface smoothness of the PEDOT:PSS layer over the Al electrode with a changing thickness of the ITO layer. Fig. 3a shows the PEDOT:PSS film on the bare Al electrode and exhibits a root mean square (RMS) roughness of about 2.4 nm. With 5 nm ITO interlayer modification of the Al electrode, the RMS roughness of the PEDOT:PSS film is drastically reduced to 1.4 nm, as seen in Fig. 3b. Comparison of the surface roughness of the PEDOT:PSS film on the bare Al, suggests that the wettability of

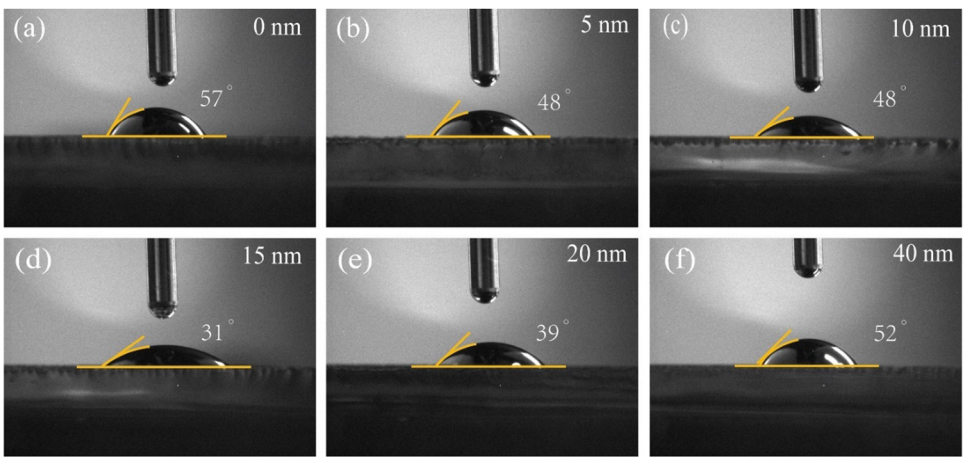

Fig. 2 Contact angle images of PEDOT:PSS solution on the Al films with varying thickness of ITO interlayer.

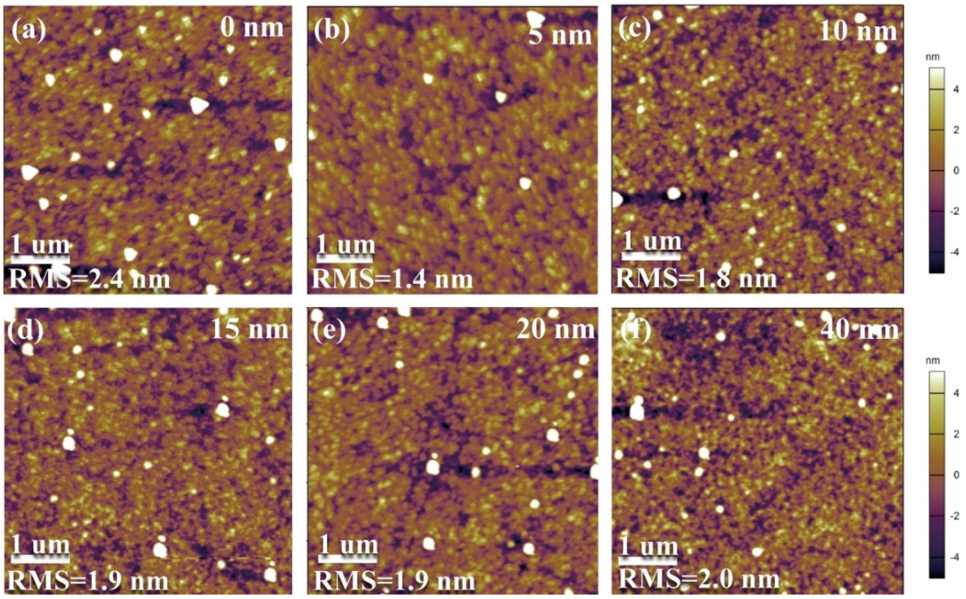

Fig. 3 AFM surface morphology images of solution-processed PEDOT:PSS film on the Al surfaces with different thicknesses of the ITO interlayer.

the Al electrode is significantly improved by interfacial treatment of the ITO layer. However, when the thickness of the ITO interlayer continuously increases from 10 nm to 40 nm, the roughness of the PEDOT:PSS film increases slightly from 1.8 nm to 2.0 nm, as shown in Fig. 3c–f. Although the increasing thickness of the ITO interlayer would increase the roughness of the PEDOT:PSS film to some extent, it is still better than that of the bare Al electrode, consistent with the contact angle measurement.

To illustrate the influence of the ITO interface modification layer on the performance of devices, the TE-QLEDs with a series of ITO thicknesses were prepared. Fig. 4a shows the current density (J)–voltage (V)–luminance (L) characteristics of the red-emitting TE-QLEDs with 0, 5, 10, or 20 nm of the ITO layer. The turn-on voltage of the devices without ITO interlayer is about 4.9 V, which also shows lower current density and luminance at the region of greater than 5 V. This suggests the formation of an Al_2O_3 insulating layer on the Al electrode after UVO treatment. With the introduction of the ITO interlayer, the current density increases greatly and the turn-on voltage of the TE-QLEDs rapidly reduces to about 1.7 V as expected, demonstrating the

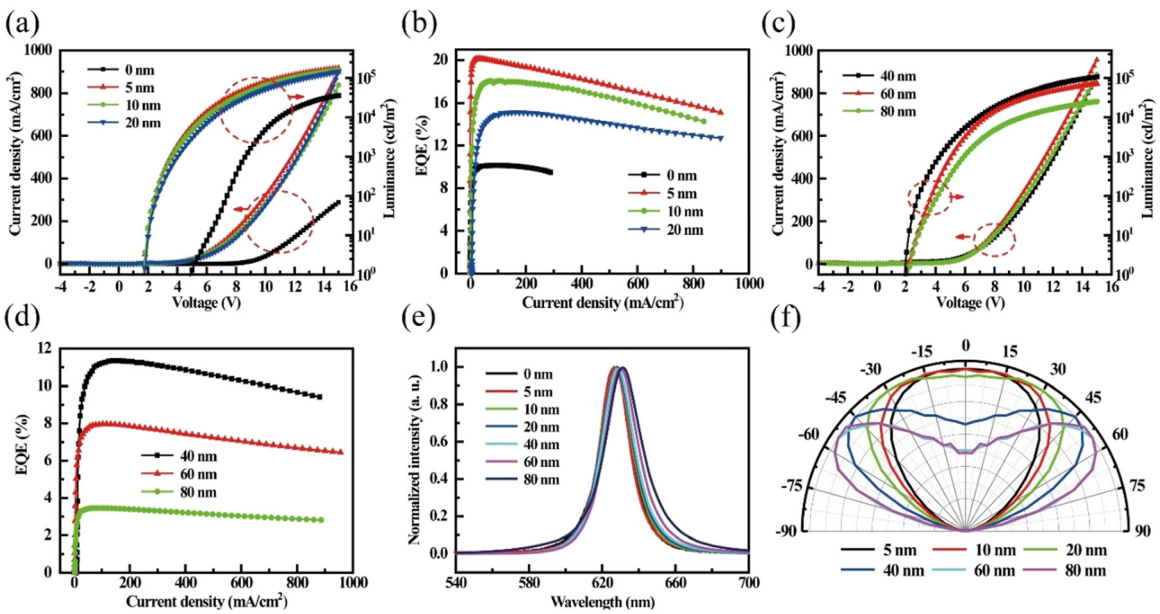

Fig. 4 (a) EQE–J, (b) J–V–L characteristics of the TE-QLEDs with 0, 5, 10 and 20 nm ITO interlayer. (c) EQE–J, (d) J–V–L characteristics of the TE-QLEDs with 40, 60 and 80 nm ITO interlayer. (e) The normalized EL spectrum and (f) Angular emission pattern of the devices with different thicknesses of ITO interlayer.

effective radiative recombination of carriers. It is worth mentioning that the maximum luminance has been improved to 175 000 cd m^{-2} (ITO = 5 nm), which is nearly five times higher than that of the device without ITO interlayer. As the thickness of ITO further increases to 10 and 20 nm, the maximum luminance at the driving voltage of 15 V decreases to 157 200 and 145 000 cd m^{-2} respectively. The introduction of the ITO interface modification layer results in a significant improvement in the performance of devices, as shown in Fig. 4b. The TE-QLEDs with 5 nm ITO interlayer display a maximum current efficiency (CE) of 26 cd A^{-1} (Fig. S2, ESI†) and a highest peak EQE of 20.1%, which is twice that of the device lacking the ITO interlayer. This high efficiency and brightness are attributed to the balance of carrier injection and the reasonable cavity length of the device. The photograph of the fabricated TE-QLEDs with 5 nm ITO interlayer driven at 4 V demonstrates high color purity and bright red emission (Fig. S3b, ESI†). However, when the thickness of the ITO interlayer increases from 10 nm to 20 nm, the maximum EQE of the device is 18% and 15.1%, respectively, as shown in Fig. 4b. The EQE and luminance of the device decrease probably owing to the destructive interference microcavity with a thicker ITO interlayer, because the destructive interference suppresses the light outcoupling from the top electrode and the photons are limited in the waveguide mode. To verify our speculation, the thickness of the ITO interlayer was further increased from 40 nm to 80 nm, and the EQE and brightness of the TE-QLEDs reduces sharply as seen in Fig. 4c and d. This result implies that the thickness change of the ITO interlayer significantly modifies the microcavity interference. The operational T_{50} lifetime of TE-QLEDs based on 5 nm ITO layer was measured to be 471.5 h at an initial luminance of 2200 cd m^{-2} (Fig. S3a, ESI†), equivalent to over 122 000 h at 100 cd m^{-2} by assuming an acceleration factor of 1.8.[35,36]

The EL spectrum of the TE-QLEDs lacking an ITO interlayer is depicted in Fig. 4e with a peak wavelength of 627 nm and a full width at half maximum (FWHM) of 20 nm (ultraviolet-visible absorption and normalized PL spectra of red QDs can be seen in Fig. S4, ESI†). The EL spectrum of TE-QLEDs gradually red-shifted to 631 nm with increasing the ITO interlayer from 5 nm to 80 nm. Simultaneously, the FWHM of devices also slightly increases to 24 nm, which originates from the changes in their cathode-to-anode distance.[37] The Commission Internationale de l'Eclairage (CIE) chromaticity coordinate diagram provides a clearer way to observe the shift of the EL spectrum when changes the thickness of the ITO layer, as shown in Fig. S5 (ESI†). These results suggest that the resonant wavelength of the TE-QLEDs exceeds the emission peak of the films.[38] The details about TE-QLEDs performance with and without ITO interlayer are summarized in Table 1. The microcavity resonance effect of our TE-QLEDs can be confirmed by the angular emission pattern plotted in Fig. 4f. The angular emission distribution of the TE-QLEDs with 5 nm and 10 nm ITO interlayer is closer to the standard Lambertian pattern, indicating that the emission is mainly in the normal direction due to the enhanced constructive interference. With increasing thickness of ITO interlayer over 20 nm, the emission of the devices is suppressed in the normal direction and forced to escape from off-axis directions, so that the devices exhibit relatively lower forward brightness and EQE, as depicted in Fig. 4c and d. Therefore, the interference effects can be modified by manipulating the thickness of the ITO interlayer, dramatically altering the optical properties and overall performance of the TE-QLEDs.

Table 1 The performance of the TE-QLEDs with varying thickness of the ITO interlayer

ITO (nm)	V_{on} (V)	EL peak (nm)	FWHM (nm)	L_{max} (cd m^{-2})	CE_{max} (cd A^{-1})	EQE_{max} (%)
w/o	4.9	627	20	35 980	13.3	10.1
5	1.7	627	20	175 000	26	20.1
10	1.7	627	20	157 200	23.7	18
20	1.7	627	20	145 000	19.1	15.1
40	1.9	628	21	105 300	14.3	11.3
60	2.0	630	22	71 570	9.2	7.9
80	2.1	631	24	25 370	3.5	3.4

To validate our claim of the microcavity effects, we performed optical simulations using semiconducting thin-film optics simulation (SETFOS) software to analyze the light outcoupling of the devices. The simulation results clearly show that the efficiency of TE-QLEDs decreases with increasing thickness of the ITO interlayer, suggesting that devices have an obvious optical cavity effect. In our device, there is wide-angle interference for the light generated inside the devices.[17,39] Interference arises within the cavity when the directly emitted light and reflected light from the bottom electrode with the same wavevector overlap, as shown in Fig. S6 (ESI†). The resonance conditions are established by

$$\frac{2\pi}{\lambda} 2n\, d_1 \cos\theta + \Phi_{bottom} = m2\pi$$

where n is the refractive index of the functional layers, λ is resonance wavelength, Φ_{bottom} is the phase shift of the Al bottom electrodes, d_1 is the distance between the emitting center and the Al bottom electrode. When the resonant wavelength of the cavity matches the emission wavelength of the film, the constructive interference occurs, leading to enhanced emission from the devices. On the contrary, the emission can be suppressed from the microcavity due to destructive interference. The resonance wavelength of the cavity can be regulated by changing the thickness d_1, which can be realized by adjusting the thickness of the ITO interlayer. The microcavity thus can explain the spectra redshifts and the change of emission direction in devices (Fig. 4e and f). As the ITO thickness increases from 40 to 80 nm, the emission wavelengths do not satisfy the constructive resonant conditions in the outcoupling direction. Furthermore, it is noted that the cavity length is controlled by the ITO interlayer, while the appropriate thickness of the carrier transport layer can ensure the balance of carrier injection.

The contributions from the different optical modes in red TE-QLEDs have been calculated and shown in Fig. 5a, and the major optical channels are described in Fig. 5b. The oscillation of the direct emission part clearly indicates that the thickness variation of the ITO interlayer significantly alters the TE-QLED

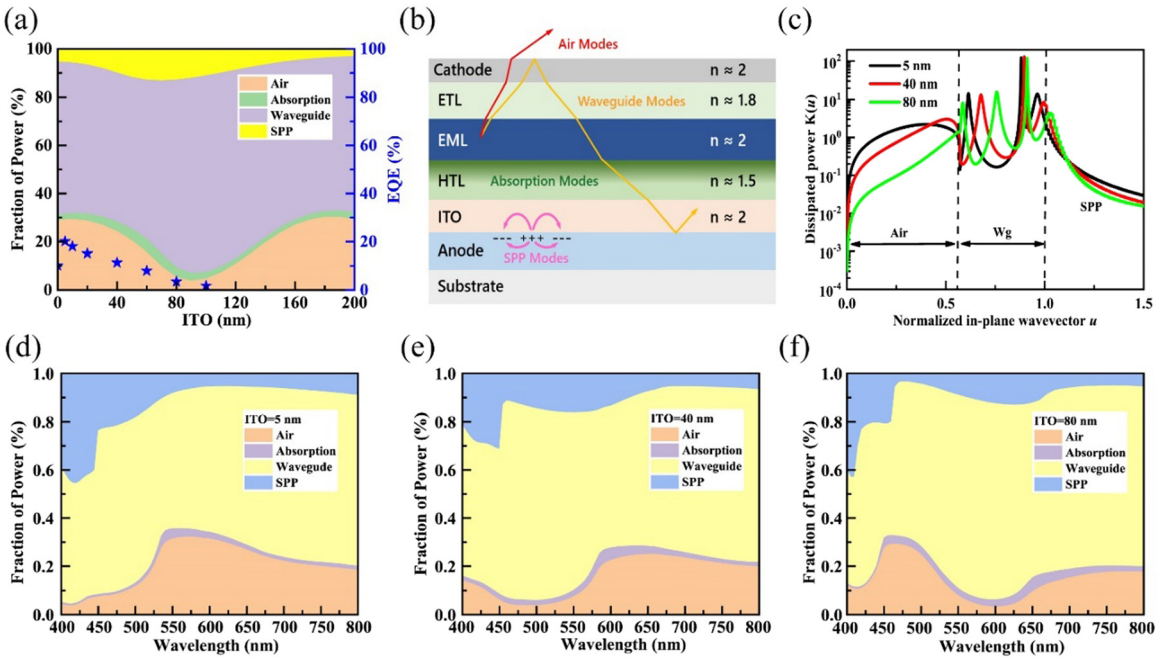

Fig. 5 (a) Changing the proportions of different optical channels by tuning the ITO interlayer thickness for the TE-QLEDs by the SETFOS software. In addition, the experimental data of TE-QLEDs are compared with the simulation results of the device. (b) Schematic diagram of optical channels with TE-QLEDs. (c) Power dissipation spectra at λ = 627 nm of devices. The wavelength-dependent optical power distribution of the TE-QLEDs with (d) 5 nm, (e) 40 nm and (f) 80 nm ITO interlayer.

cavity. When the ITO is 2 nm, the air mode reaches 29.4% of all optical channels. While the ITO changes to 90 nm, the air mode has been rapidly suppressed to only 3.7% but the waveguide mode of the devices will be enhanced. This means that the waveguide mode competes with the air mode (outcoupled light) primarily. More energy is transferred from the air mode to the waveguide mode as the thickness of the ITO interlayer increases, resulting in degraded performance of the TE-QLEDs. Our simulation model's validity is confirmed by the good agreement between the simulation results and the experimental data. To further investigate, we compare the power dissipation spectra calculated for the TE-QLEDs with 5 nm, 40 nm, and 80 nm ITO interlayer at the wavelength of 627 nm. Fig. 5c demonstrates that the waveguide mode transitions from three peaks to four peaks when increasing the thickness of the ITO interlayer. Furthermore, the waveguide peaks exhibit a shift as the thickness of ITO layer increases, and the emission of the devices in the normal direction is suppressed due to the destructive interference. Fig. 5d–f illustrate the wavelength-dependent optical power distribution of the TE-QLEDs with 5 nm, 40 nm and 80 nm ITO interlayers. It clearly manifests that the optimal TE-QLEDs with a 5 nm ITO layer exhibit a significantly lower waveguide and SPP losses, and the outcoupling efficiency of the TE-QLEDs reaches 30% at the resonance wavelength of 627 nm, which is the highest among the devices. Experiments and simulations have shown that utilizing ITO as the interface modification layer is an effective technique for TE-QLEDs. This approach not only improves the balance of carrier injection in the devices but also ensures optimal outcoupling efficiency of the TE-QLEDs.

Conclusion

In summary, highly bright and efficient TE-QLEDs have been designed and fabricated by a solution process, in which ITO of different thicknesses is employed as an interfacial layer on the Al surface. With an optimized thickness of the ITO interlayer, a uniform PEDOT:PSS film is spin-coated over the Al electrode, which effectively improves the hole injection. Simultaneously, the height of the cavity in the TE-QLEDs is controlled by the thickness of the ITO interlayer. The thickness of the interlayer plays a crucial role in controlling the optical properties of the devices. By optimizing the ITO interfacial layer, the red-emitting TE-QLEDs can achieve a maximum brightness and EQE of 175 000 cd m^{-2} and 20.1%, respectively. It should be noted that the efficiency of the device is strongly influenced by the thickness of the ITO layer, which is consistent with the optical simulations.

Conflicts of interest

There are no conflicts of interest to declare.

Acknowledgements

We would like to acknowledge support from China Postdoctoral Science Foundation (No. 2021M702243), Guangdong Department of Science and Technology and Hongkong Innovation and Technology Fund under grant (No. 2021A0505110015), Shenzhen Science and Technology Program (No. KQTD20170810105439418), the National Natural Science Foundation of China (No. 62005114,

22005198), National Key Research and Development Program of China (No. 2021YFB3602703, 2022YFB3606504, and 2022YFB 3602903), and Shenzhen Key Laboratory for Advanced Quantum Dot Displays and Lighting (No. ZDSYS201707281632549).

References

1 V. L. Colvin, M. C. Schlamp and A. P. Alivisatos, *Nature*, 1994, **370**, 354–357.
2 A. P. Alivisatos, *Science*, 1996, **271**, 933–937.
3 C. Dang, L. Lee, C. Breen, J. S. Steckel, S. Coe-Sullivan and A. Nurmikko, *Nat. Nanotechnol.*, 2012, **7**, 335–339.
4 X. Li, Y.-B. Zhao, F. Fan, L. Levina, M. Liu, R. Quintero-Bermudez, X. Gong, L. N. Quan, J. Fan, Z. Yang, S. Hoogland, O. Voznyy, Z.-H. Lu and E. H. Sargent, *Nat. Photonics*, 2018, **12**, 159–164.
5 W. Cao, C. Xiang, Y. Yang, Q. Chen, L. Chen, X. Yan and L. Qian, *Nat. Commun.*, 2018, **9**, 2608.
6 Y. Yang, Y. Zheng, W. Cao, A. Titov, J. Hyvonen, J. R. Manders, J. Xue, P. H. Holloway and L. Qian, *Nat. Photonics*, 2015, **9**, 259–266.
7 Q. Sun, Y. A. Wang, L. S. Li, D. Wang, T. Zhu, J. Xu, C. Yang and Y. Li, *Nat. Photonics*, 2007, **1**, 717–722.
8 Q. Wu, F. Cao, S. Wang, Y. Wang, Z. Sun, J. Feng, Y. Liu, L. Wang, Q. Cao, Y. Li, B. Wei, W.-Y. Wong and X. Yang, *Adv. Sci.*, 2022, **9**, 2200959.
9 Z. Sun, Q. Wu, S. Wang, F. Cao, Y. Wang, L. Li, H. Wang, L. Kong, L. Yan and X. Yang, *ACS Appl. Mater. Interfaces*, 2022, **14**, 15401–15406.
10 X. Dai, Z. Zhang, Y. Jin, Y. Niu, H. Cao, X. Liang, L. Chen, J. Wang and X. Peng, *Nature*, 2014, **515**, 96–99.
11 Y. Deng, F. Peng, Y. Lu, X. Zhu, W. Jin, J. Qiu, J. Dong, Y. Hao, D. Di, Y. Gao, T. Sun, M. Zhang, F. Liu, L. Wang, L. Ying, F. Huang and Y. Jin, *Nat. Photonics*, 2022, **16**, 505–511.
12 J. Song, O. Wang, H. Shen, Q. Lin, Z. Li, L. Wang, X. Zhang and L. S. Li, *Adv. Funct. Mater.*, 2019, **29**, 1808377.
13 Q. Wu, X. Gong, D. Zhao, Y.-B. Zhao, F. Cao, H. Wang, S. Wang, J. Zhang, R. Quintero-Bermudez, E. H. Sargent and X. Yang, *Adv. Mater.*, 2022, **34**, 2108150.
14 L. Kong, J. Wu, Y. Li, F. Cao, F. Wang, Q. Wu, P. Shen, C. Zhang, Y. Luo, L. Wang, L. Turyanska, X. Ding, J. Zhang, Y. Zhao and X. Yang, *Sci. Bull.*, 2022, **67**, 529–536.
15 B. Geffroy, P. L. Roy and C. Prat, *Polym. Int.*, 2006, **55**, 572–582.
16 S. Chen, L. Deng, J. Xie, L. Peng, L. Xie, Q. Fan and W. Huang, *Adv. Mater.*, 2010, **22**, 5227–5239.
17 G. Liu, X. Zhou and S. Chen, *ACS Appl. Mater. Interfaces*, 2016, **8**, 16768–16775.
18 X. Yang, E. Mutlugun, C. Dang, K. Dev, Y. Gao, S. T. Tan, X. W. Sun and H. V. Demir, *ACS Nano*, 2014, **8**(8), 8224–8231.
19 T. Lee, D. Hahm, K. Kim, W. K. Bae, C. Lee and J. Kwak, *Small*, 2019, **15**, 1905162.
20 H. Li, S. Zhou and S. Chen, *Laser Photonics Rev.*, 2023, **17**, 2300371.
21 M. Lu, J. Guo, S. Sun, P. Lu, J. Wu, Y. Wang, S. V. Kershaw, W. W. Yu, A. L. Rogach and Y. Zhang, *Nano Lett.*, 2020, **20**, 2829–2836.
22 R. H. Friend, R. W. Gymer, A. B. Holmes, J. H. Burroughes, R. N. Marks, C. Taliani, D. D. C. Bradley, D. A. Dos Santos, J. L. Bredas, M. Logdlund and W. R. Salaneck, *Nature*, 1999, **397**, 121–128.
23 Q. W. Liu, S. Yuan, S. Q. Sun, W. Luo, Y. J. Zhang, L. S. Liao and M. K. Fung, *J. Mater. Chem. C*, 2019, **7**, 4344–4349.
24 J. Krantz, K. Forberich, P. Kubis, F. Machui, J. Min, T. Stubhan and C. J. Brabec, *Org. Electron.*, 2015, **17**, 334–339.
25 H. Ma, H. L. Yip, F. Huang and A. K. Y. Jen, *Adv. Funct. Mater.*, 2010, **20**, 1371–1388.
26 X. Yang, E. Mutlugun, Y. Zhao, Y. Gao, K. S. Leck, Y. Ma, L. Ke, S. T. Tan, H. V. Demir and X. W. Sun, *Small*, 2014, **10**, 247–252.
27 F. Cao, H. Wang, P. Shen, X. Li, Y. Zheng, Y. Shang, J. Zhang, Z. Ning and X. Yang, *Adv. Funct. Mater.*, 2017, **27**, 1704278.
28 Y. Jiang, S. Chen and H.-S. Kwok, *SID Symp. Dig. Tech. Pap.*, 2017, **48**, 161–164.
29 Z. Tang, J. Lin, L. Wang, Y. Lv, Y. Hu, Y. Fan, X. Guo, J. Zhao, Y. Wang and X. Liu, *J. Mater. Chem. C*, 2017, **5**, 9138–9145.
30 S. Ding, W. Wang, X. Xiao, X. Qu, Z. Wu, B. Xu, S. Chen, K. Wang and X. W. Sun, *AIP Adv.*, 2020, **10**, 065308.
31 L. Shi and S. Chen, *ACS Appl. Mater. Interfaces*, 2022, **14**, 30039–30045.
32 H. Zhang and S. Chen, *J. Mater. Chem. C*, 2019, **7**, 2291–2298.
33 H. J. Snaith, H. Kenrick, M. Chiesa and R. H. Friend, *Polymer*, 2005, **46**, 2573–2578.
34 K. Sugiyama, H. Ishii, Y. Ouchi and K. Seki, *J. Appl. Phys.*, 2000, **87**, 295–298.
35 H. Yu, H. Zhu, M. Xu, J. Zhang, H. Feng, L. Zhang, S. Liu and W. Xie, *ACS Photonics*, 2023, **10**, 2192–2200.
36 T. Lee, B. J. Kim, H. Lee, D. Hahm, W. K. Bae, J. Lim and J. Kwak, Bright and Stable Quantum Dot Light-Emitting Diodes, *Adv. Mater.*, 2022, **34**, 2106276.
37 H. Riel, S. Karg, T. Beierlein, B. Ruhstaller and W. Rieß, *Appl. Phys. Lett.*, 2003, **82**, 466–468.
38 A. Dodabalapur, L. J. Rothberg, R. H. Jordan, T. M. Miller, R. E. Slusher and J. M. Phillips, *J. Appl. Phys.*, 1996, **80**, 6954–6964.
39 G. Mei, W. Wang, D. Wu, P. A. Surman, K. Wang, W. C. H. Choy, X. Yang, W. Xu and X. W. Sun, *IEEE Photonics J.*, 2022, **14**, 8219709.

